

Tuning of p–n–p-Type Conduction in AgCuS through Cation Vacancy: Thermopower and Positron Annihilation Spectroscopy Investigations

Moinak Dutta,[†] Dirtha Sanyal,^{‡,§} and Kanishka Biswas^{*,†}

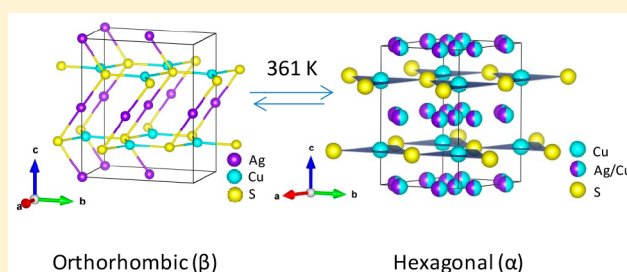
[†]New Chemistry Unit, Jawaharlal Nehru Centre for Advanced Scientific Research (JNCASR), Jakkur P.O., Bangalore 560064, India

[‡]Variable Energy Cyclotron Centre, 1/AF Bidhannagar, Kolkata 700064, India

[§]Homi Bhabha National Institute, Anushakti Nagar, Mumbai 400094, India

Supporting Information

ABSTRACT: Understanding the complex phenomenon behind the structural transformations is a key requisite to developing important solid-state materials with better efficacy such as transistors, resistive switches, thermoelectrics, etc. AgCuS, a superionic semiconductor, exhibits temperature-dependent p–n–p-type conduction switching and a colossal jump in thermopower during an orthorhombic to hexagonal superionic transition. Tuning of p–n–p-type conduction switching in superionic compounds is fundamentally important to realize the correlation between electronic/phonon dispersion modulation with changes in the crystal structure and bonding, which might contribute to the design of better thermoelectric materials. Herein, we have created extrinsic Ag/Cu nonstoichiometry in AgCuS, which resulted in the vanishing of p–n–p-type conduction switching and improved its thermoelectric properties. We have performed the selective removal of cations and measured their temperature-dependent thermopower and Hall coefficient, which demonstrates only p-type conduction in the Ag_{1–x}CuS and AgCu_{1–x}S samples. The removal of Cu is much more efficient in arresting conduction switching, whereas in the case of Ag vacancy, p–n–p-type conduction switching vanishes at higher vacant concentrations. Positron annihilation spectroscopy measurements have been done to shed further light on the mechanisms behind this structural transition-dependent conduction switching. Cation (Ag⁺/Cu⁺) nonstoichiometry in AgCuS significantly increases the vacancy concentration, hence, the p-type carriers, which is confirmed by positron annihilation spectroscopy and Hall measurement. The Ag_{1–x}CuS and AgCu_{1–x}S samples exhibit ultralow thermal conductivity (~0.3–0.5 W/m·K) in the 290–623 K temperature range because of the low-energy cationic sublattice vibration that arises as a result of the movement of loosely bound Ag/Cu within the stiff S sublattice.



INTRODUCTION

Structural phase transformation remains one of the most intriguing phenomena for modern-day inorganic and solid-state chemistry, primarily because it acts as a podium for furnishing materials with a plethora of novel physical properties,¹ viz., superconductivity,² superionic conduction,^{3–6} the photoelectronic effect,^{7,8} optical storage,⁹ giant magnetoresistance,¹⁰ p–n- and p–n–p-type conduction switching,^{3,11–15} and thermoelectricity.^{6,16–20} Apart from changes in the crystal structure, phase transformation also leads to changes in the orientation of electron clouds, which, in turn, influences their spin states. These deformations result in the evolution of electronic structures and phonon dispersions. Among these novel attributes, temperature-dependent p–n–p-type conduction switching is relatively unexplored and can potentially find its usage in temperature-controlled diode and transistor devices, which can operate efficiently and reversibly near room temperature.²¹

Silver and copper chalcogenides, chalcogenides, and halides have garnered interest over the past few years because of their tendency to exhibit mixed ionic and electronic conduction in superionic phases.^{3,4,13,22} These compounds are composed of cationic and anionic substructures that are weakly coupled. Structural transition of these compounds leads to a superionic phase at high temperatures, which can primarily be attributed to the formation of a substructure of mobile cations. AgCuS belongs to this family and shows several temperature-dependent structural transitions.^{13,23} Recently, we have shown that AgCuS undergoes p–n–p-type conduction switching coupled with a colossal change of thermopower in the vicinity of an orthorhombic to hexagonal structural transition.¹³ The switching of the conduction type can be attributed to the change in the electronic structure and Ag vacancy concentration during the first superionic structural transition at ~360

Received: May 7, 2018

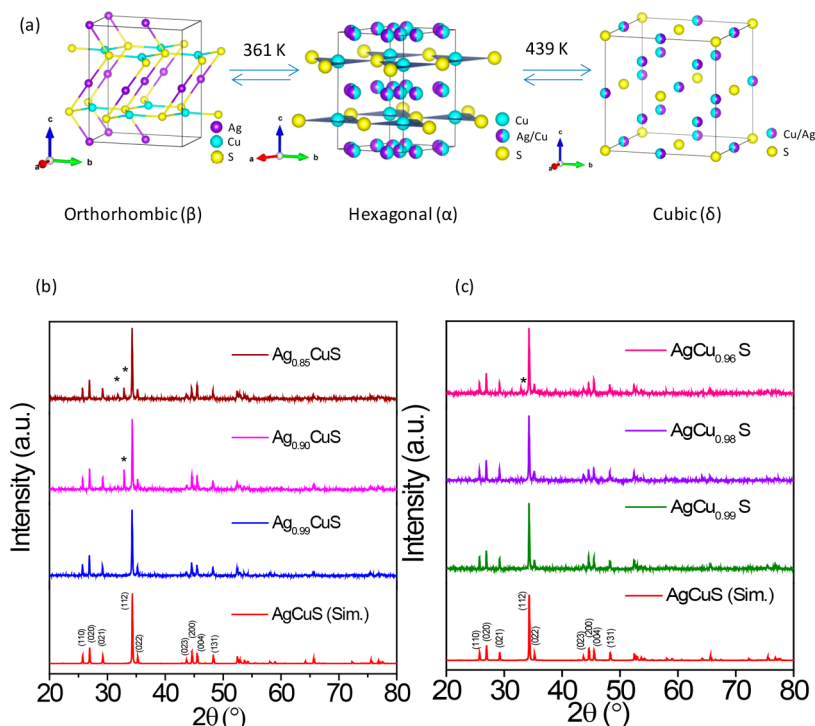


Figure 1. (a) Temperature-driven structural transformations for AgCuS. AgCuS undergoes phase transition from an ordered orthorhombic phase to a partially cation-disordered hexagonal phase to finally a fully cation-disordered cubic phase. (b and c) Powder XRD patterns for the different Ag- and Cu-deficient AgCuS, respectively. Extra peak(s) (marked by asterisks) at higher deficiencies is (are) due to the presence of Cu_2S .

K. The room temperature orthorhombic phase β -AgCuS ($Cmc2_1$) is composed of distorted hexagonal-close-packing (hcp) S atoms (Figure 1a).²³ The Cu atoms lie within the distorted hcp S layer and form a three-coordinated structure. Ag atoms form a loosely bound face-centered-cubic (fcc) framework, alternating with those of CuS, which are bonded to two S atoms with near-linear geometry (Figure 1a).²⁴ Hexagonal (α phase at 361 K) and cubic (δ phase at 439 K) are high-temperature superionic phases with space groups $P6_3/mmc$ and $Fm\bar{3}m$, respectively. AgCuS undergoes structural phase transformations at 361 K ($\beta \rightarrow \alpha$) and further at 439 K ($\alpha \rightarrow \delta$). The high-temperature hexagonal (α) phase is composed of partially disordered Ag and Cu, with S atoms preserving the hcp sublattice (Figure 1a).²⁴ The cubic (δ phase) phase is the other high-temperature structure, where all of the cations (Ag^+/Cu^+) are randomly distributed at the tetrahedral and octahedral sites of the rigid fcc S sublattice (Figure 1a).²⁴ In general, the anion sublattice is crystalline, while the cation mobilizes with an increase in the temperature, akin to liquidlike disorder within the crystalline chalcogenide/chalcohalide framework, which leads to p–n- and p–n–p-type conduction switching and important thermoelectric properties in AgCuS, AgCuSe, $\text{Ag}_{10}\text{Te}_4\text{Br}_3$, and AgBiSe_2 .^{10,12–14}

Tuning of p–n–p-type conduction switching in superionic compounds is fundamentally important to realize the correlation between electronic/phonon dispersion modulation with changes in the crystal structure and bonding, which might contribute to the design of better thermoelectric materials. Recently, tuning of p–n–p-type conduction switching in AgCuS has been performed by reducing the grain size to nanoscale, which opens up the band gap and increases the Ag vacancy concentration, thereby altering the conduction switching.²⁵ Interestingly, in AgBiSe_2 , p–n–p-type conduction switching vanishes for its bulk counterpart.¹⁷ The crystallite

size here plays a prominent role in conduction switching because it modifies the electronic structure. Tuning of conduction switching has also been seen in anion-substituted $\text{Ag}_{10}\text{Te}_4\text{Br}_3$,²⁶ where substitution influences the carrier transport and electronic structure, which leads to a shift in the phase transition temperature. p-type conduction in β -AgCuS is the result of intrinsic Ag vacancy, which provides an effective path for Ag^+ -ion migration during superionic phase transition.¹³ The presence of hybridized Cu–S orbitals in the intermediate semimetallic electronic structure state contributes to n-type conduction, which is responsible for the p–n–p-type conduction switching in AgCuS.¹³ The purposeful creation of nonstoichiometry or cation (Ag^+/Cu^+) vacancy may result in a change in the p–n–p-type conduction switching in AgCuS. The findings will not only help us to gain insight into the pertinent mechanism for the conduction switching but also show its usefulness in the development of better thermoelectric materials.

Herein, we demonstrate an innovative way to tune p–n–p-type conduction in AgCuS, while trying to keep the grain size intact. The Ag vacancy concentration and Cu–S hybridized states are pivotal for p–n–p-type conduction switching in AgCuS. Thus, we intentionally created extrinsic Ag and Cu vacancies in AgCuS in order to tune the conduction switching. In the case of Ag vacancies, p–n–p-type conduction switching vanishes at $\text{Ag}_{0.85}\text{CuS}$, whereas for Cu, p–n–p vanishes even at only 1 mol % Cu vacant samples. The nature of the vacancy and relative concentrations with increasing respective cation (Ag^+/Cu^+) nonstoichiometry in AgCuS has been analyzed by the positron annihilation lifetime (PAL) and shape (S) parameter. An increase in the PAL and an increase in the S parameter with respect to pristine AgCuS with increasing Ag^+/Cu^+ vacancy concentration indicate enhancement of the p-type carrier in nonstoichiometric AgCuS, which was also further confirmed by

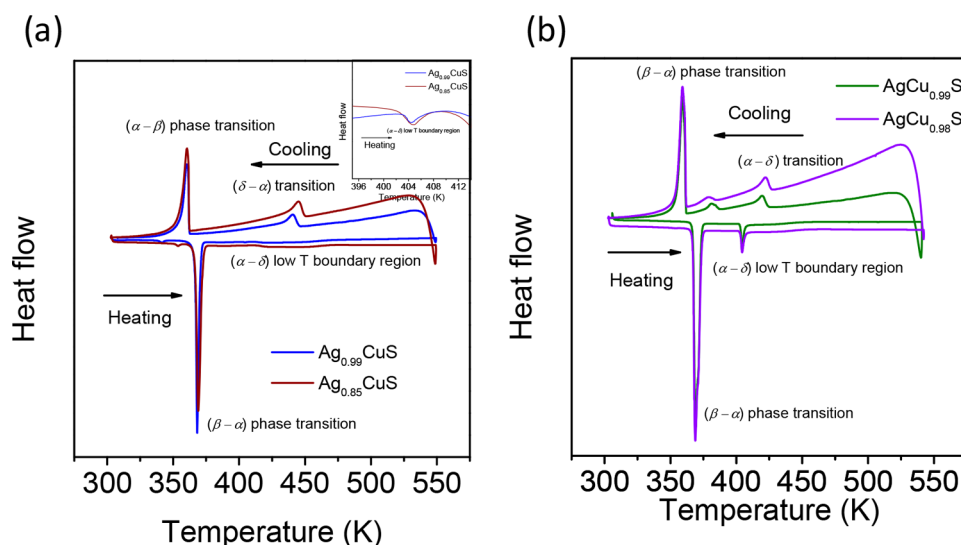


Figure 2. DSC curves for (a) Ag_{1-x}CuS ($x = 0.01$ and 0.15) and (b) AgCu_{1-x}S ($x = 0.01$ and 0.02). There is no apparent shift in the phase transition temperature in any of the vacant samples. The inset of part a contains zoomed-in versions of hexagonal to cubic phase transitions around 404 K.

the Hall measurement at room temperature. A change in the thermopower (ΔS) during an orthorhombic to hexagonal superionic transition decreases with increasing cation deficiency. The superionic phase transition temperature is independent of vacancy concentrations in AgCuS, which is confirmed by differential scanning calorimetry (DSC) analysis. All of the samples exhibit ultralow thermal conductivity (~ 0.3 – 0.5 W/m·K) in the temperature region of 290–623 K, which is due to the dynamic movement of the cations within the rigid anion sublattice. Ag_{0.85}CuS exhibits a maximum thermoelectric figure of merit (zT) of ~ 0.15 , which is significantly higher than that of pristine AgCuS.

EXPERIMENTAL SECTION

Starting Materials. Elemental Ag ($\geq 99.99\%$, Sigma-Aldrich), Cu (99.999% , Alfa Aesar), and S (99.999% , Alfa Aesar) were used in stoichiometric amounts for the synthesis of the compounds. They were used as obtained, and no further purification was done.

Synthesis. Ingots (~ 7 g) of Ag_{1-x}CuS ($x = 0.01, 0.1, \text{ and } 0.15$), and AgCu_{1-x}S ($x = 0.01, 0.02, \text{ and } 0.04$) were prepared by taking stoichiometric amounts of Ag, Cu, and S. They were transferred to quartz ampules and subsequently flame-sealed under high vacuum ($\sim 10^{-5}$ Torr). These vacuum-sealed ampules were then slowly heated up to 773 K over 12 h to minimize any S evaporation, then gradually heated to 1223 K in 5 h followed by soaking for 24 h, and finally air-quenched to room temperature. Each ingot was subsequently cut and polished into a parallelepiped ($\sim 2 \times 3 \times 8$ mm³) and thin-coin-shaped (8 mm diameter and 2 mm thick) samples to perform electrical transport and thermal diffusivity measurements, respectively.

Powder X-ray Diffraction (XRD). The samples were finely ground using an agate mortar and were used for powder XRD. Powder XRD was done under room temperature conditions using Cu $K\alpha$ radiation source ($\lambda = 1.5406$ Å) on a Bruker D8 diffractometer. Temperature-dependent powder XRD was carried out using a Rigaku Smart-lab X-ray diffractometer, with the radiation source being Cu $K\alpha$ ($\lambda = 1.5406$ Å). The temperature ramp rate during heating and cooling cycles was kept at 5 K/min with an additional 2 min for steadying the temperature. The scanning rate was kept at 1°/min.

Seebeck Coefficient and Electrical Conductivity. The Seebeck coefficients and electrical conductivities of the samples were measured from room temperature to 550 K under He atmosphere using an ULVAC-RIKO ZEM-3 instrument.

Thermal Conductivity. Thin-coin-shaped samples were used for thermal diffusivity (D) measurements in a Netzsch LFA 457

instrument under N₂ atmosphere. The total thermal conductivity was then calculated using the equation $\kappa_{\text{total}} = DC_p\rho$, where ρ is the density of the measured samples. C_p is the heat capacity, which is obtained using the reference pyroceram. All of the samples have densities greater than 96% of the theoretical density.

Hall Measurement. Parallelepiped-shaped samples were used for Hall measurements. The measurement was carried out in an in-house setup developed by Excel Instruments, using a varying magnetic field of 0.0–0.57 T and a direct current of 50 mA. For high-temperature measurements, the ramp rate was kept at a steady 1 K/min, with a fluctuation limit of 1 K during the measurements.

DSC. Finely powdered samples were used for DSC measurements. The measurements were carried out on a TA DSCQ2000 instrument with a heating rate of 5 K/min within the temperature range 290–550 K.

Positron Annihilation Spectroscopy (PAS). PAS measurements have been carried out using a ²²NaCl source (strength ~ 10 μCi) and sealed in a thick Ni foil (1.5 μm). The sealed source has been placed amidst two identical plane-faced samples (8 mm diameter \times 1 mm thick pellet) for both the PAL and Doppler broadening (DB) measurements. The PAL have been calculated with a conventional fast–fast coincidence assembly, which is comprised of two γ -ray detectors (25 mm long and 25 mm tapered to 13 mm diameter BaF₂ scintillator, optically coupled with an XP2020 Q photomultiplier tube) and two differential discriminators having constant fraction (Fast ComTech; model 7029A), which has a time resolution (full width at half-maximum) of ~ 220 ps measured by the prompt γ -ray of a ⁶⁰Co source. Approximately 10 million coincidence counts have been detected and recorded in a multichannel analyzer. The recorded lifetime spectrum has been examined using the computer code PATFIT-88 with proper source corrections. A DB of positron annihilation radiation (DBPAR) experiment has been carried out at room temperature by a single HPGe detector (efficiency, 12%; type, PGC 1216 sp; DSG, Germany), which has an energy resolution of 1.15 at 514 keV of ⁸⁵Sr. The DBPAR spectra have been recorded in a dual-ADC-based multiparameter data acquisition system (MPA-3 of FAST ComTec, Germany). The DR of annihilation at 511 keV γ -ray spectra has been examined by evaluating the line-shape parameter (S parameter).^{27,28} The S parameter is defined as the ratio of counts in the central area under the photopeak ($|511 \text{ keV} - E_i| \leq 0.85 \text{ keV}$) to the whole area under the photopeak ($|511 \text{ keV} - E_i| \leq 4.25 \text{ keV}$). The S parameter mainly tells us about the fraction of positrons that are being annihilated by the lower momentum electrons with reference to the total electrons annihilated. The contribution of the S parameter is crucial because of the occurrence of open-volume defects, where the positrons get annihilated.

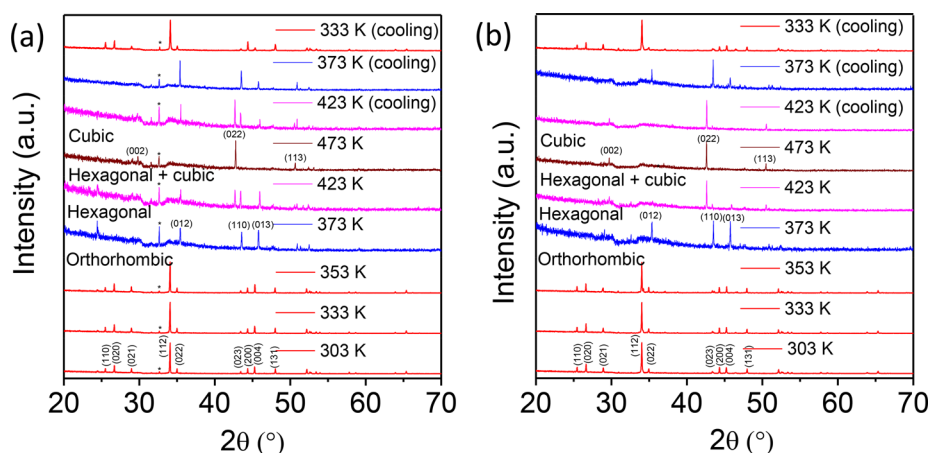


Figure 3. Temperature-dependent heating and cooling powder XRD data for (a) $\text{Ag}_{0.85}\text{CuS}$ and (b) $\text{AgCu}_{0.98}\text{S}$. Both samples show reversible phase transitions. The peak marked with an asterisk (*) in part a is due to the presence of a Cu_2S second phase.

RESULTS AND DISCUSSION

Nonstoichiometric $\text{Ag}_{1-x}\text{CuS}$ ($x = 0.01, 0.1,$ and 0.15) and $\text{AgCu}_{1-x}\text{S}$ ($x = 0.01, 0.02,$ and 0.04) were synthesized by a vacuum-sealed tube melting reaction of Ag, Cu, and S. Parts b and c of Figure 1 show the powder XRD patterns of $\text{Ag}_{1-x}\text{CuS}$ ($x = 0.01, 0.1,$ and 0.15) and $\text{AgCu}_{1-x}\text{S}$ ($x = 0.01, 0.02,$ and 0.03) samples, respectively. The samples were found to procure an orthorhombic β - AgCuS structure ($Cmc2_1$) in low concentration of Ag/Cu vacancy. When the Ag/Cu vacancy concentration is increased significantly, we observe a minute second phase of Cu_2S ($P4_32_12$, marked by asterisks in Figure 1b,c) along with β - AgCuS . It has been observed that, for both cation (Ag^+/Cu^+)-deficient samples, interestingly Cu_2S gets isolated as the minor second phase, where the common perception is that, in the case of $\text{AgCu}_{1-x}\text{S}$, Ag_2S or elemental Ag should contribute to any second phase.

Further, a temperature-dependent structural transition in nonstoichiometric $\text{Ag}_{1-x}\text{CuS}$ ($x = 0.01$ and 0.15) and $\text{AgCu}_{1-x}\text{S}$ ($x = 0.01$ and 0.02) has been studied via DSC measurement (Figure 2a,b). The heating curve of DSC shows a strong peak around 369 K, which corresponds to the first high-temperature orthorhombic to hexagonal ($\beta \rightarrow \alpha$) phase transition. The peak around 404 K could be attributed to the low-temperature boundary region for the second high-temperature hexagonal to cubic ($\alpha \rightarrow \delta$) phase transition.²³ Although in hindsight the $\alpha \rightarrow \delta$ transition shows no peak in the Ag-deficient $\text{Ag}_{1-x}\text{CuS}$, zoomed in the versions of $\text{Ag}_{0.99}\text{CuS}$ and $\text{Ag}_{0.85}\text{CuS}$, the DSC data around 404 K suggests that there is a presence of the $\alpha \rightarrow \delta$ transition peak (Figure 2a, inset). The DSC data further provide information that there is no shift in the transition temperature with varying vacancy concentration. This finding is of fundamental interest because it shows, unlike $\text{Ag}_{10}\text{Te}_4\text{Br}_3$, where the transition temperature shifts with anion substitution;²⁶ here the transition is immune to vacancies. The presence of a peak at 369 K depicts that the phase transition does take place in all of the samples, but with an increase of the Ag vacancy in $\text{Ag}_{1-x}\text{CuS}$, which imparts p-type conduction, the formation of semimetallic states is not enough for a change in the conduction switching. In the case of the $\text{AgCu}_{1-x}\text{S}$ samples, although the $\beta \rightarrow \alpha$ transition takes place at around 369 K, as shown in the DSC plot, the absence of Cu–S hybridized bonds becomes a contributing factor for the tuning of p–n–p-type conduction switching. The cooling data show a peak around 440 K for $\text{Ag}_{1-x}\text{CuS}$ and 425 K for $\text{AgCu}_{1-x}\text{S}$. These peaks can

be attributed to the $\alpha \rightarrow \delta$ phase transition. The peak at around 380 K is a two-phase boundary region of the $\alpha \rightarrow \delta$ transition. The region between the aforementioned two peaks (425 and 380 K) in the cooling cycle contains both hexagonal (α) and cubic (δ) forms.

To further corroborate the DSC findings, temperature-dependent powder XRD has also been carried out to provide conclusive evidence of the phase transition taking place in the cation vacant samples. We have performed temperature-dependent powder XRD for two samples, i.e., $\text{Ag}_{0.85}\text{CuS}$ and $\text{AgCu}_{0.98}\text{S}$ (Figure 3a,b). The presence of different phases with changes in the temperature provides us with conclusive proof of the phase transformations in these cation vacant samples. For both samples, we have observed temperature-dependent phase transitions from orthorhombic (room temperature) to hexagonal (~ 370 K) to a mixture of hexagonal and cubic (~ 423 K) to finally a fully cubic phase. The heating and cooling cycles prove that the phase transitions in cation (Ag^+/Cu^+) vacant AgCuS samples are reversible in nature, which do complement our DSC results. For the Ag vacant sample (i.e., $\text{Ag}_{0.85}\text{CuS}$), we observe the presence of a minor second Cu_2S phase, which does not undergo any noticeable phase transition within the measured temperature range.

The p-type conduction in the orthorhombic phase is due to the intrinsic Ag vacancies, which acts as an effective route for the hopping of Ag^+ ions to these inherent vacant positions.¹³ Here, we have extrinsically created Ag vacancies by using stoichiometric amounts of Ag, Cu, and S in the appropriate ratio to form compounds with the nominal composition of $\text{Ag}_{1-x}\text{CuS}$ ($x = 0.01, 0.1,$ and 0.15). The motive behind this was to create more vacancies for the Ag^+ ions to migrate to, which may tune the conduction switching property in AgCuS . Because it has already been understated that Ag vacancies are responsible for p-type conduction in β - AgCuS at room temperature, creating more such vacancies will lead to predominantly p-type conduction throughout the temperature range. We have measured the carrier type and concentrations of $\text{Ag}_{1-x}\text{CuS}$ samples by Hall coefficient measurement at room temperature (Table 1). Pristine AgCuS exhibits a p-type carrier concentration of $1.3 \times 10^{15} \text{ cm}^{-3}$, which significantly increases to $1.27 \times 10^{17} \text{ cm}^{-3}$ in $\text{Ag}_{0.9}\text{CuS}$.

Figure 4a shows the temperature-dependent thermopower (S) for the $\text{Ag}_{1-x}\text{CuS}$ samples. The room temperature Seebeck coefficient value decreases from $719 \mu\text{V/K}$ in pristine AgCuS to

Table 1. Carrier Concentrations for the Different Cation (Ag^+ and Cu^+) Vacant Compounds^a

sample	carrier concentration (cm^{-3})
AgCuS	1.3×10^{15}
$\text{Ag}_{0.99}\text{CuS}$	1.09×10^{16}
$\text{Ag}_{0.90}\text{CuS}$	1.27×10^{17}
$\text{Ag}_{0.85}\text{CuS}$	1.02×10^{17}
$\text{AgCu}_{0.99}\text{S}$	7.11×10^{15}
$\text{AgCu}_{0.98}\text{S}$	9.26×10^{15}
$\text{AgCu}_{0.96}\text{S}$	5.37×10^{15}

^aAll of the measurements are done at room temperature.

378 $\mu\text{V}/\text{K}$ for $\text{Ag}_{0.85}\text{CuS}$ (Figure 4c). Such a decrease in the thermopower with an increase in the Ag vacancy concentration in $\text{Ag}_{1-x}\text{CuS}$ can be attributed to the increase in the p-type carrier concentrations (Table 1). With an initial increase in the temperature, the thermopower increases gradually, followed by a sudden colossal jump ($\Delta S = 1737 \mu\text{V}/\text{K}$), accompanying with it a change in the conduction type from p to n during an orthorhombic to hexagonal superionic transition ($\sim 367 \text{ K}$) in pristine AgCuS. Upon a further increase in the temperature, the thermopower reverts back to the p type and stays p type afterward. With a gradual increment in Ag vacancy, the change

in the thermopower (ΔS) during the superionic phase transition decreases (Figure 4c). This decrease in the change of the ΔS value can be attributed to an increase in the p-type carrier (Table 1), which nullifies some of the effective n-type carriers during the phase transition. For the $\text{Ag}_{0.85}\text{CuS}$ sample, the absence of such p–n–p-type conduction switching is observed and the compound remains predominantly p-type throughout the measured temperature. Although there is a slight drop in the thermopower at the vicinity of the $\beta \rightarrow \alpha$ phase transition, the drop is not sufficient enough to cause a change in the conduction type. The hump around 450 K in the thermopower value for $\text{Ag}_{0.85}\text{CuS}$ is most likely due to the pronounced effect of $\alpha \rightarrow \alpha + \delta$ to finally a fully δ phase transition, which is present in other samples also but the hump is not as prominent as that of $\text{Ag}_{0.85}\text{CuS}$, which is not clear at this moment. Thus, we were able to tune the p–n–p-type conduction switching in AgCuS to fully p-type conduction via nonstoichiometric $\text{Ag}_{1-x}\text{CuS}$.

We have conducted temperature-dependent Hall measurements for both the pristine AgCuS and $\text{Ag}_{0.85}\text{CuS}$ samples. We have seen a similar trend in the sign of the Hall coefficient (R_{H}), which gives an indication regarding the nature of the conduction in the material. In the case of pristine AgCuS, R_{H} is initially positive (p-type conduction), then changes to negative

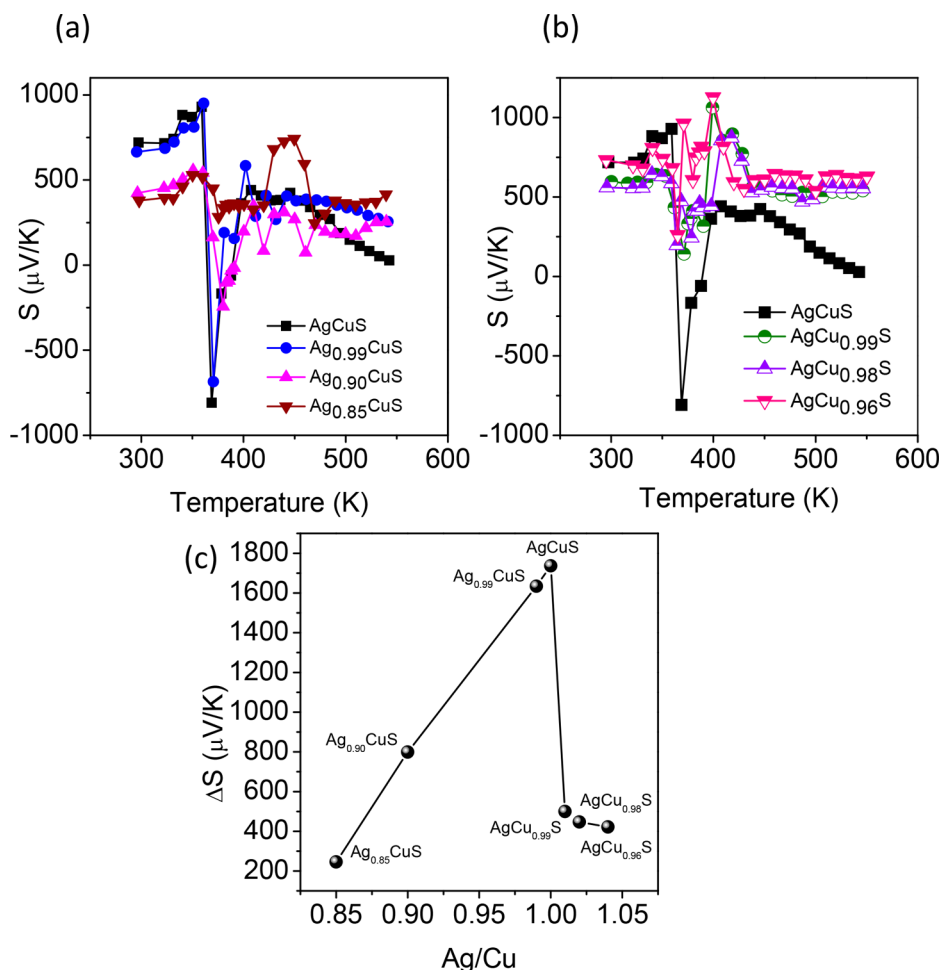


Figure 4. Temperature-dependent Seebeck coefficient values for (a) $\text{Ag}_{1-x}\text{CuS}$ (where $x = 0, 0.01, 0.1, 0.15$). The p–n–p-type conduction switching is tuned and eliminated at $x = 0.15$. Temperature-dependent Seebeck coefficient values for (b) $\text{AgCu}_{1-x}\text{S}$ (where $x = 0, 0.01, 0.02, 0.04$). Here the p–n–p-type conduction switching vanished at low deficiencies only. (c) Change in the thermopower (ΔS) versus vacancy concentration. ΔS decreases with increasing vacancy.

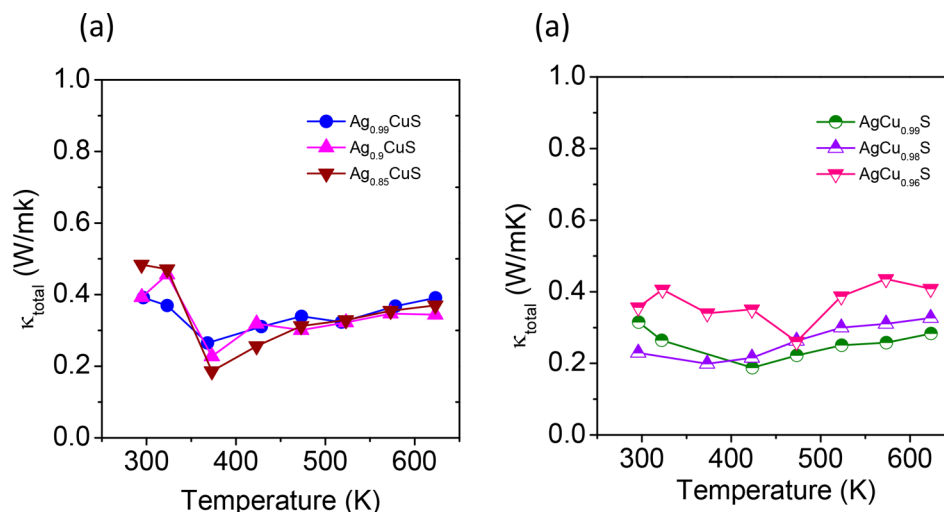


Figure 5. Temperature-dependent total thermal conductivity plots for (a) Ag-deficient $\text{Ag}_{1-x}\text{CuS}$ samples and (b) Cu-deficient $\text{AgCu}_{1-x}\text{S}$ samples.

(n-type) during the $\beta \rightarrow \alpha$ phase transition, and reverts back to a positive value (p-type). In the case of cation vacant $\text{Ag}_{0.85}\text{CuS}$, the R_{H} remains positive (p-type) within the measurement range, indicating that $\text{Ag}_{0.85}\text{CuS}$ is a fully p-type conductor (Figure S1a,b), which supports the temperature-dependent Seebeck coefficient data. The temperature-dependent carrier concentration data are given in Tables S1 and S2.

Hybridized Cu–S orbitals in AgCuS forms the semimetallic intermediate electronic state during $\beta \rightarrow \alpha$ transition, which provides n-type conduction at ~ 365 K.¹³ To understand the role of Cu vacancy, we extrinsically created Cu vacant samples using stoichiometric amounts of Ag, Cu, and S in the appropriate ratio to form compounds with the nominal composition of $\text{AgCu}_{1-x}\text{S}$ ($x = 0.01, 0.02,$ and 0.04). Interestingly, Cu nonstoichiometry does not increase much the p-type carrier concentration of $\text{AgCu}_{1-x}\text{S}$ compared to that of Ag vacant samples (Table 1). For example, the p-type carrier concentration of $5.37 \times 10^{15} \text{ cm}^{-3}$ was obtained in $\text{AgCu}_{0.96}\text{S}$, which is much lower compared to that of $\text{Ag}_{1-x}\text{CuS}$.

Figure 4b shows the temperature-dependent thermopower (S) for the $\text{AgCu}_{1-x}\text{S}$ samples. Unlike the Ag vacant samples, where the tuning of the conduction switching was possible to attain only at higher vacancy (e.g., $\text{Ag}_{0.85}\text{CuS}$), here we observed complete loss of p–n–p-type conduction switching at lower Cu vacancies, i.e., in $\text{AgCu}_{0.99}\text{S}$. This can be attributed to the fact that the hybridized Cu–S states are the prime factor for the formation of an n-type semimetallic electronic state during the $\beta \rightarrow \alpha$ phase transition, which can be perturbed by creating a small amount of Cu vacancy. Moreover, a partial density of states in the electronic structure clearly showed that the Cu 3d orbital resides near the Fermi level during p–n-type conduction switching,¹³ making the contribution from Cu toward the conduction switching much more prevalent than its Ag counterpart in $\text{Ag}_{1-x}\text{CuS}$. Because the Cu 3d orbitals reside so close to the Fermi level, a small perturbation in them might hinder overlapping of the valence and conduction bands during the phase transition, which actually makes $\text{AgCu}_{1-x}\text{S}$ a fully p-type semiconductor. Typically, $\text{AgCu}_{0.96}\text{S}$ exhibits a S value of $733 \mu\text{V/K}$ at room temperature, remains p-type throughout, and has a S value of $630 \mu\text{V/K}$ at 550 K. Here the change is the thermopower with increasing vacancy is much more gradual. The ΔS value for $\text{AgCu}_{0.99}\text{S}$ is $500 \mu\text{V/K}$, which decreases gradually to $422 \mu\text{V/K}$ for $\text{AgCu}_{0.96}\text{S}$ (Figure 4c). The

temperature-dependent Hall coefficient data of $\text{AgCu}_{0.96}\text{S}$ are also consistent with the observed Seebeck coefficient, which confirms that $\text{AgCu}_{0.96}\text{S}$ is indeed a fully p-type semiconductor (Figure S1c). The temperature-dependent carrier concentration data are given in Table S3.

Although the presence of a minor second phase of Cu_2S in nonstoichiometric AgCuS could contribute to tuning of the p–n–p transition because a significant amount of it is present in high cation (Ag^+/Cu^+) vacant samples, it is to be noted that, in $\text{AgCu}_{0.90}\text{S}$, the presence of Cu_2S does not inhibit the change in the conduction type. In the case of $\text{AgCu}_{0.99}\text{S}$, p–n–p-type conduction switching vanishes, although no such Cu_2S phase is observed. Thus, the presence of Cu_2S might not play a profound role in the tuning of p–n–p-type conduction switching.

The $\text{Ag}_{1-x}\text{CuS}$ ($x = 0.01, 0.1,$ and 0.15) and $\text{AgCu}_{1-x}\text{S}$ ($x = 0.01, 0.02,$ and 0.04) samples exhibit ultralow thermal conductivity (κ_{total}) of $0.3\text{--}0.5 \text{ W/m}\cdot\text{K}$ in the $290\text{--}623 \text{ K}$ range, which is slightly lower than that of pristine AgCuS (Figure 5). The total thermal conductivity is given as a summation of both the electrical and lattice thermal conductivity ($\kappa_{\text{total}} = \kappa_{\text{lattice}} + L\sigma T$, where L is the Lorentz number). Because the electrical conductivity of the samples is very low (Figure S2), the total conductivity is effectively comprised of the lattice thermal conductivity (κ_{lattice}). A rational explanation for such a low thermal conductivity is probably due to the effective phonon scattering by the mobile cations, which shows dynamic disorder inside the rigid S sublattice. With an increase of the vacancy, the relative ease of hopping increases, which might be the possible reason for having a lower thermal conductivity than that of pristine AgCuS. Also, the previous first-principle calculations on AgCuS provide us with a phonon dispersion plot, which reveals a distinct separation of the two energy modes.¹³ The low-lying phonon modes are primarily constituted of loosely bound cations. This low-lying acoustic phonon mode is indicative of the softness of AgCuS and, hence, the low thermal conductive nature. Because electron transport is governed predominantly by the rigid S sublattice and the low thermal conductivity is due to a loosely bound cation sublattice, an effective decoupling has been observed between the electrical and phonon transport in AgCuS, which is essential for thermoelectrics. With an increase in the vacancy, the electrical conductivity also increases because of the apparent

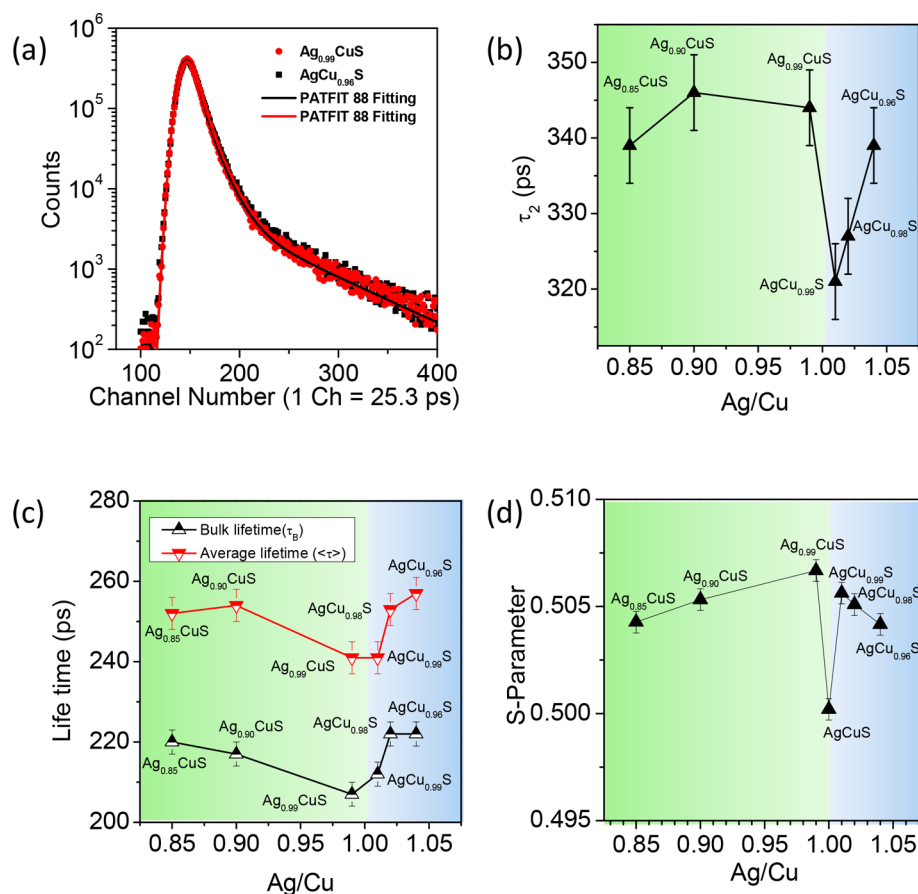


Figure 6. (a) PAL spectrum for Ag_{0.99}CuS (red dots) and AgCu_{0.96}S (black dots). The red and black fitting lines are used to obtain different lifetime components for the two samples, respectively. Vacancy-dependent (b) τ_2 values due to the formation of positronium at larger voids, (c) average lifetime ($\langle\tau\rangle$), and bulk lifetime (τ_B). (d) Variation of the DBPAR line-shape parameter (*S* parameter in PAS) with the stoichiometric ratio of Ag and Cu (Ag/Cu) in AgCuS.

increase in the p-type carrier concentration (Table 1), which results in a thermoelectric figure of merit (zT) of ~ 0.15 at 445 K for the Ag_{0.85}CuS sample. For the AgCu_{0.96}S sample, a zT value of ~ 0.12 is achieved at 400 K. The zT values of ~ 0.15 in Ag_{0.85}CuS and ~ 0.12 in AgCu_{0.96}S are significantly higher than that of pristine AgCuS ($zT \sim 0.025$), which is due to tuning of p–n–p-type conduction switching (Figure S3).

PAS has been a cornerstone in recent history for characterizing and identifying the chemical nature of the defects in different solids.^{12,13,27–30} The PAL and DB measurements of the Ag_{1–*x*}CuS and AgCu_{1–*x*}S samples are the two principle techniques; one probes the electron density distribution, while the other probes the electron momentum distribution in the studied material. Structural phase transitions in different sulfide samples using these two positron annihilation techniques have been studied successfully.^{13,25}

We have characterized all of the as-synthesized samples (Ag_{0.85}CuS, Ag_{0.90}CuS, Ag_{0.99}CuS, AgCu_{0.99}S, AgCu_{0.98}S, and AgCu_{0.96}S) by positron lifetime spectroscopy and DBPAR spectroscopy. The entire lifetime spectrum has been analyzed by the PATFIT-88 program with proper source correction. The best fit of the spectrum (variance of fit of <1 per channel) is with three lifetime component fittings, having a long lifetime of 1.3 ns with 4% intensity. This lifetime component is due to the formation of positronium at the surfaces or at the void spaces inside the sample. Figure 6a represents the PAL spectrum for the Ag_{0.99}CuS and AgCu_{0.96}S samples. The shortest lifetime

component (τ_1) of about 156 ps is attributed to the free annihilation of the positron. The intermediate lifetime component (τ_2) is due to the positron annihilation at defect sites. In the present studies, the intermediate lifetime (τ_2) components are in the range of 321 ± 5 – 347 ± 5 ps with relative intensities of 43–53%.

Figure 6b represents the variation of τ_2 with the stoichiometric ratio of Ag and Cu (i.e., Ag/Cu) in the AgCuS sample. It was already observed earlier that, for a high-quality crystalline ingot of AgCuS, the value of τ_2 is about 272 ps and had been identified as the Ag vacancy.¹³ It is interesting that τ_2 is minimal around Ag/Cu ~ 1 . With decreasing Ag/Cu ratio to values of less than unity, τ_2 there is a gradual increase from 343 ps for Ag_{0.99}CuS to 346 ps for Ag_{0.90}CuS and then a slight decrease to 339 ps for Ag_{0.85}CuS, while the increment of τ_2 is relatively faster in the case of the Cu vacant samples (320 ps for AgCu_{0.99}S to 339 ps for AgCu_{0.96}S). The increase of τ_2 suggests the agglomeration of cation defects at a particular defect site and hence increases of positron lifetime value, which indicates toward an increase in the cation vacancy in the Ag_{1–*x*}CuS and AgCu_{1–*x*}S samples. The intensity of the intermediate positron lifetime (I_2), which is directly proportional to the defect concentration, is also plotted for all of the samples (Figure S4). This also suggests that the cation defect concentration is more when the stoichiometry is changed in either way. The average and bulk positron lifetimes were further calculated using the formula $\langle\tau\rangle = (\tau_1 I_1 + \tau_2 I_2)/(I_1 + I_2)$ and τ_B

$= (I_1/\tau_1 + I_2/\tau_2)^{-1}(I_1 + I_2)$, respectively, and plotted against the stoichiometry as Figure 6c. The nature of both graphs are similar, and as is typical, the value of τ_B is more than $\langle\tau\rangle$, indicating the presence of a vacancy defect in the sample, which increases with increasing nonstoichiometry in AgCuS, which has a significant impact on the vanishing p–n–p-type conduction switching in the Ag_{1-x}CuS and AgCu_{1-x}S samples.

The DBPAR line-shape parameter, S (defined in the Experimental Section), provides us with a quantitative idea about the number of positrons being annihilated with the lower momentum valence electrons. Figure 6d shows variation of the S parameter of the different samples plotted against their stoichiometry. With the corresponding increase of the vacancies (due to the change of the stoichiometry, i.e., Ag_{1-x}CuS or AgCu_{1-x}S), the S -parameter value increases drastically compared to that of pristine AgCuS and then it varies only slightly with an increase in the vacancy concentration in nonstoichiometric samples. The initial drastic increase in the S parameter in the nonstoichiometric sample is due to the formation of vacancies, which is expected.²⁷ The consequent slight change in the S parameter in cation vacant samples can be ascribed to the saturation trapping of positrons, which can be activated with even a few atomic percent of vacancies. The lifetime (τ_2) values of the cation (Ag⁺/Cu⁺) vacant samples are in the range of 320–345 ps, which can mainly be attributed to the formation of vacancy clusters, unlike the lifetime of pristine AgCuS (~272 ps), which is mainly due to the innate Ag vacancies. The I_2 (%) plot against cation (Ag⁺/Cu⁺) vacancies (Figure S4) shows the increase in the cation defect concentration with an increase in the vacancy. The slight decrease in the S parameter for nonstoichiometric samples can thus be a combination of certain factors along with cation-vacancy-like formation of vacancy clusters, saturation trapping, and diffusion of positrons to grain boundaries.

CONCLUSIONS

Cation (Ag⁺ and Cu⁺) vacancies in AgCuS tune the temperature-dependent p–n–p-type conduction switching, and the samples remain p-type, which indeed improves the thermoelectric performance. Cu nonstoichiometry proved to be more detrimental to the p–n–p-type conduction switching than Ag vacancies. Cu nonstoichiometry disrupts the hybridized Cu–S orbitals, which are pivotal for the formation of an intermediate n-type semimetallic state and subsequent electronic band overlap, which is the key for p–n–p-type conduction switching in AgCuS. Thus, the vacancy-induced disappearance of p–n–p-type conduction switching can be due to a combination of a couple of contributing factors: (a) excess Ag vacancies, which impart p-type conduction to the material, and (b) perturbation of the Cu–S n-type semimetallic state by the formation of Cu nonstoichiometry, which enables compounds to remain p-type throughout the measured temperature range. Ag⁺/Cu⁺ vacancy increases the p-type carrier concentration, which provides a boost to electrical transport. Further, the Ag_{1-x}CuS and AgCu_{1-x}S samples demonstrate ultralow thermal conductivity due to low-energy soft phonons arising from the hopping of cations within the rigid anion sublattice.

ASSOCIATED CONTENT

Supporting Information

The Supporting Information is available free of charge on the ACS Publications website at DOI: 10.1021/acs.inorgchem.8b01246.

Figures for temperature-dependent Hall coefficient, electrical conductivity, and thermoelectric figure of merit (zT), an I_2 (%) plot, and tables for the temperature-dependent carrier concentrations of selected samples (PDF)

AUTHOR INFORMATION

Corresponding Author

*E-mail: kanishka@jncasr.ac.in.

ORCID

Dirtha Sanyal: 0000-0003-2490-3610

Kanishka Biswas: 0000-0001-9119-2455

Notes

The authors declare no competing financial interest.

ACKNOWLEDGMENTS

The work was also partially supported by the DAE-BRNS YSRA project [Grant 37(3)/20/01/2015/BRNS] and Sheikh Saqr Laboratory. M.D. thanks the University Grants Commission for a research fellowship. The authors also thank Prof. Rajeev Ranjan (IISc, Bangalore) and his Ph.D. scholar Arnab De for their help in carrying out the temperature-dependent powder XRD experiment at their laboratory.

REFERENCES

- (1) Rao, C. N. R. Phase transitions and the chemistry of solids. *Acc. Chem. Res.* **1984**, *17*, 83–89.
- (2) Coronado, E.; Marti-Gastaldo, C.; Navarro-Moratalla, E.; Ribera, A.; Blundell, S. J.; Baker, P. J. Coexistence of superconductivity and magnetism by chemical design. *Nat. Chem.* **2010**, *2*, 1031–6.
- (3) Guin, S. N.; Biswas, K. Temperature driven p–n–p type conduction switching materials: current trends and future directions. *Phys. Chem. Chem. Phys.* **2015**, *17*, 10316–25.
- (4) Keen, D. A. Disordering phenomena in superionic conductors. *J. Phys.: Condens. Matter* **2002**, *14*, R819.
- (5) Olvera, A. A.; Moroz, N. A.; Sahoo, P.; Ren, P.; Bailey, T. P.; Page, A. A.; Uher, C.; Poudeu, P. F. P. Partial indium solubility induces chemical stability and colossal thermoelectric figure of merit in Cu₂Se. *Energy Environ. Sci.* **2017**, *10*, 1668–1676.
- (6) Liu, H.; Shi, X.; Xu, F.; Zhang, L.; Zhang, W.; Chen, L.; Li, Q.; Uher, C.; Day, T.; Snyder, G. J. Copper ion liquid-like thermoelectrics. *Nat. Mater.* **2012**, *11*, 422–5.
- (7) Zhang, Q.; Liu, Y.; Bu, X.; Wu, T.; Feng, P. A rare (3,4)-connected chalcogenide superlattice and its photoelectric effect. *Angew. Chem., Int. Ed.* **2008**, *47*, 113–6.
- (8) Liu, Y.; Lin, Q.; Zhang, Q.; Bu, X.; Feng, P. Visible-Light-Driven, Tunable, Photoelectrochemical Performance of a Series of Metal-Chelate, Dye-Organized, Crystalline, CdS Nanoclusters. *Chem. - Eur. J.* **2014**, *20*, 8297–8301.
- (9) Ohkoshi, S.; Tsunobuchi, Y.; Matsuda, T.; Hashimoto, K.; Namai, A.; Hakoe, F.; Tokoro, H. Synthesis of a metal oxide with a room-temperature photoreversible phase transition. *Nat. Chem.* **2010**, *2*, 539–45.
- (10) Ishiwata, S.; Shiomi, Y.; Lee, J. S.; Bahramy, M. S.; Suzuki, T.; Uchida, M.; Arita, R.; Taguchi, Y.; Tokura, Y. Extremely high electron mobility in a phonon-glass semimetal. *Nat. Mater.* **2013**, *12*, 512–7.
- (11) Nilges, T.; Lange, S.; Bawohl, M.; Deckwart, J. M.; Janssen, M.; Wiemhofer, H. D.; Decourt, R.; Chevalier, B.; Vannahme, J.; Eckert, H.; Wehrich, R. Reversible switching between p- and n-type

conduction in the semiconductor $\text{Ag}_{10}\text{Te}_4\text{Br}_3$. *Nat. Mater.* **2009**, *8*, 101–8.

(12) Xiao, C.; Qin, X.; Zhang, J.; An, R.; Xu, J.; Li, K.; Cao, B.; Yang, J.; Ye, B.; Xie, Y. High thermoelectric and reversible *p-n-p* conduction type switching integrated in dimetal chalcogenide. *J. Am. Chem. Soc.* **2012**, *134*, 18460–6.

(13) Guin, S. N.; Pan, J.; Bhowmik, A.; Sanyal, D.; Waghmare, U. V.; Biswas, K. Temperature dependent reversible *p-n-p* type conduction switching with colossal change in thermopower of semiconducting AgCuS . *J. Am. Chem. Soc.* **2014**, *136*, 12712–20.

(14) Shi, Y.; Assoud, A.; Sankar, C. R.; Kleinke, H. $\text{Ti}_2\text{Ag}_{12}\text{Se}_7$: A New pnp Conduction Switching Material with Extraordinarily Low Thermal Conductivity. *Chem. Mater.* **2017**, *29*, 9565–9571.

(15) Han, C.; Sun, Q.; Cheng, Z. X.; Wang, J. L.; Li, Z.; Lu, G. Q.; Dou, S. X. Ambient Scalable Synthesis of Surfactant-Free Thermoelectric CuAgSe Nanoparticles with Reversible Metallic-*n-p* Conductivity Transition. *J. Am. Chem. Soc.* **2014**, *136*, 17626–17633.

(16) Zhao, L. D.; Lo, S. H.; Zhang, Y.; Sun, H.; Tan, G.; Uher, C.; Wolverton, C.; Dravid, V. P.; Kanatzidis, M. G. Ultralow thermal conductivity and high thermoelectric figure of merit in SnSe crystals. *Nature* **2014**, *508*, 373–7.

(17) Pan, L.; Berardan, D.; Dragoe, N. High thermoelectric properties of *n*-type AgBiSe_2 . *J. Am. Chem. Soc.* **2013**, *135*, 4914–7.

(18) Guin, S. N.; Biswas, K. Cation Disorder and Bond Anharmonicity Optimize the Thermoelectric Properties in Kinetically Stabilized Rocksalt AgBiS_2 Nanocrystals. *Chem. Mater.* **2013**, *25*, 3225–3231.

(19) Guin, S. N.; Srihari, V.; Biswas, K. Promising thermoelectric performance in *n*-type AgBiSe_2 : effect of aliovalent anion doping. *J. Mater. Chem. A* **2015**, *3*, 648–655.

(20) Guin, S. N.; Banerjee, S.; Sanyal, D.; Pati, S. K.; Biswas, K. Origin of the Order-Disorder Transition and the Associated Anomalous Change of Thermopower in AgBiS_2 Nanocrystals: A Combined Experimental and Theoretical Study. *Inorg. Chem.* **2016**, *55*, 6323–6331.

(21) Janek, J. The bridge to redox switches. *Nat. Mater.* **2009**, *8*, 88.

(22) Lange, S.; Nilges, T. $\text{Ag}_{10}\text{Te}_4\text{Br}_3$: A New Silver(I) (poly)-Chalcogenide Halide Solid Electrolyte. *Chem. Mater.* **2006**, *18*, 2538–2544.

(23) Trots, D. M.; Senyshyn, A.; Mikhailova, D. A.; Knapp, M.; Baetz, C.; Hoelzel, M.; Fuess, H. High-temperature thermal expansion and structural behaviour of stromeyerite, AgCuS . *J. Phys.: Condens. Matter* **2007**, *19*, 136204.

(24) Santamaria-Perez, D.; Morales-Garcia, A.; Martinez-Garcia, D.; Garcia-Domene, B.; Muhle, C.; Jansen, M. Structural phase transitions on AgCuS stromeyerite mineral under compression. *Inorg. Chem.* **2013**, *52*, 355–61.

(25) Guin, S. N.; Sanyal, D.; Biswas, K. The effect of order–disorder phase transitions and band gap evolution on the thermoelectric properties of AgCuS nanocrystals. *Chem. Sci.* **2016**, *7*, 534–543.

(26) Osters, O.; Bawohl, M.; Bobet, J.-L.; Chevalier, B.; Decourt, R.; Nilges, T. A conceptual approach to materials for resistivity switching and thermoelectrics. *Solid State Sci.* **2011**, *13*, 944–947.

(27) Hautojärvi, P.; Corbel, C. In *Positron Spectroscopy of Solids*; Dupasquier, A., Mills, A. P., Jr., Eds.; IOS Press: Amsterdam, The Netherlands, 1995; p 491.

(28) Krause-Rehberg, R.; Leipner, H. S. *Positron Annihilation in Semiconductors*; Springer Verlag: Berlin, 1999.

(29) Sarkar, A.; Chakrabarti, M.; Ray, S. K.; Bhowmick, D.; Sanyal, D. Positron annihilation lifetime and photoluminescence studies on single crystalline ZnO . *J. Phys.: Condens. Matter* **2011**, *23*, 155801.

(30) Dhar, J.; Sil, S.; Dey, A.; Ray, P. P.; Sanyal, D. Positron Annihilation Spectroscopic Investigation on the Origin of Temperature-Dependent Electrical Response in Methylammonium Lead Iodide Perovskite. *J. Phys. Chem. Lett.* **2017**, *8*, 1745–1751.